1521-0103/370/3/843–854$35.00
THE JOURNAL OF PHARMACOLOGY AND EXPERIMENTAL THERAPEUTICS

https://doi.org/10.1124/jpet.118.254672
J Pharmacol Exp Ther 370:843–854, September 2019

Special Section on Drug Delivery Technologies

CNS Delivery and Anti-Inflammatory Effects of Intranasally Administered Cyclosporine-A in Cationic Nanoformulations[S]

Sunita Yadav, Grishma Pawar, Praveen Kulkarni, Craig Ferris, and Mansoor Amiji

Department of Pharmaceutical Sciences, School of Pharmacy, Northeastern University, Boston, Massachusetts (S.Y., G.P., C.F., M.A.); Center for Translational Neuro-Imaging, Northeastern University, Boston, Massachusetts (P.K., C.F.); and Novartis Institute of Biomedical Research, Cambridge, Massachusetts (S.Y.)

Received October 26, 2018; accepted December 10, 2018

ABSTRACT

The main objective of this study was to develop and evaluate the CNS delivery efficiency, distribution, therapeutic efficacy, and safety of cyclosporine A (CSA) using a cationic oil-in-water nanoemulsion system upon intranasal administration. An omega-3 fatty acid–rich, flaxseed oil–based nanoemulsion was used for intranasal delivery to the brain, and further magnetic resonance imaging (MRI) was used to evaluate and confirm the transport of the positively charged CSA nanoemulsion (CSA-NE) in CNS. Furthermore, the anti-inflammatory potential of CSA peptide was evaluated using the lipopolysaccharide (LPS) model of neuroinflammation in rats. CSA-NE showed a good safety profile when tested in vitro in RPMI 2650 cells. Upon intranasal administration in rats, the nanoemulsion delivery system showed higher uptake in major regions of the brain based on changes in MRI T_1 (longitudinal relaxation time) values. Additionally, CSA nanoemulsion showed improved therapeutic efficacy by inhibiting proinflammatory cytokines in the LPS-stimulated rat model of neuroinflammation compared with solution formulation. Preliminary safety evaluations show that the nanoemulsion system was well tolerated and did not cause any acute negative effects in rats. Based on these results, intranasal delivery of CSA and other "neuroprotective peptides" may provide a clinically translatable strategy for treating neurologic diseases.

Introduction

Various neurologic conditions, such as neuroinflammation, pain, psychiatric disorders, stroke, and brain cancers can benefit significantly from disease-modifying biologic therapies such as peptides and proteins (Yi et al., 2014). However, because of their inherent instability, large molecular weight, and permeability restrictions these molecules are unable to cross the blood-brain barrier upon systemic administration (Yi et al., 2014). Additionally, these molecules have rapid clearance and a short half-life in the systemic circulation (Yi et al., 2014). Although several strategies are available that include neurosurgically based delivery, such as intraventricular drug infusion, intracerebral implants, hyperosmotic opening of the blood-brain barrier, and convection-enhanced delivery to the brain, most of these strategies are highly invasive and risky strategies (Lu et al., 2014).

Cyclosporine-A (CSA), a cyclic decapeptide, is a potent immunosuppressive agent that has shown great potential as a neuroprotective agent. Because of its immunosuppressant properties of altering T lymphocyte (the inhibition of interleukin production in T cells) activity, it has been used in transplant medicine and has also been used to reduce the incidence of transplant rejection (Osman et al., 2011). CSA has also been known to play an important role as a neuroprotective agent by preventing a mitochondrial permeability transition pore and thus helps in preserving normal mitochondrial function, which can prevent strokes (Osman et al., 2011). Various in vitro and in vivo studies have demonstrated that CSA plays a role in preventing neuronal damage in models of excitotoxicity

This study was partially supported by the National Institute of Neurologic Disorders and Stroke of the National Institutes of Health through Grant R21-NS-066984.
https://doi.org/10.1124/jpet.118.254672.
[S] This article has supplemental material available at jpet.aspetjournals.org.

ABBREVIATIONS: AB, apical to basolateral; BA, basolateral to apical; CNS, central nervous system; CSA, cyclosporine A; CSA-NE, positively charged cyclosporine A nanoemulsion; CSA-S, aqueous suspension of cyclosporine A; DMSO, dimethylsulfoxide; DTPA, diethylenetriamine pentaacetic acid; FOV, field of view; Gd^{3+}, gadolinium; Gd^{3+}-NE, gadolinium-encapsulated nanoemulsion; HPLC, high-performance liquid chromatography; IL, interleukin; iNOS, inducible nitric oxide synthase; LC, liquid chromatography; LPS, lipopolysaccharide; MRI, magnetic resonance imaging; MS, mass spectrometry; MTT, 3-(4,5-dimethylthiazol-2-yl)-2,5-diphenyl tetrazolium bromide; NE-SA, positively charged cyclosporine A nanoemulsion; NE-T, negatively charged cyclosporine A nanoemulsion; PBS, phosphate-buffered saline; PCR, polymerase chain reaction; PDI, polydispersity index; PE, phosphatidylethanolamine; R_1, magnetic relaxivity; SN, substantia nigra; T_1, longitudinal relaxation time; T-CSA, cyclosporine A solution in 0.5% dimethylsulfoxide Hanks' balanced salt solution 1× buffer; TEER, transepithelial electrical resistance; TNF-α, tumor necrosis factor-α; TR, repetition time.

and also helps in the regulation of neurotransmitter release (Snyder et al., 1998; Santos and Schauwecker, 2003). CSA has also shown neuroprotective effects in various neurodegenerative diseases by inducing the production of certain neurotrophic factors (Miyata et al., 2001; Sheehan et al., 2006; Gabryel and Bozena, 2009).

However, such beneficial effects of CSA were observed only by chronic administration of the drug at a very high dose of >10 mg/kg. The higher dosing strategy leads to systemic levels of CSA that produce limiting negative side effects, such as immune suppression, hepatotoxicity, and nephrotoxicity (Göldner and Patrick, 1996; Osman et al., 2011). Hence, CSA as a potential neurotherapeutic agent has not been explored so far. Given the above obstacles in utilizing CSA as a neuroprotective agent, there has been an increased interest in developing alternative strategies for delivering CSA specifically to the brain and limiting systemic exposure.

This study was aimed at delivering CSA to the brain using the intranasal route to enhance the therapeutic anti-inflammatory effects with decreased dose and dose-related side effects. The intranasal route was used for CSA brain delivery as it is a noninvasive route of administration and takes advantage of the olfactory epithelium for brain drug delivery without any systemic exposure. Since its discovery, intranasal delivery has been used in rats (Chow et al., 2001), and in animal models of Alzheimer's disease (Jogani et al., 2008), brain tumors (Hashizume et al., 2008), epilepsy (Barakat et al., 2006), and pain (Westin et al., 2005). Intranasal administration has also been used in a few human studies (Benedict et al., 2004; Foltin and Haney, 2004; Kosfeld et al., 2005) for delivering certain biologic molecules. Most of the intranasal studies have been focused on the efficacy of therapeutic molecules, and less is known about how various formulations and molecules get distributed in the brain upon intranasal dosing (Djupesland et al., 2014). Recently, different imaging techniques have been used in the diagnosis of brain diseases. We have used magnetic resonance imaging (MRI) as a noninvasive way of characterizing the transport of the delivery system in different regions of the brain upon intranasal administration. Second, an omega-3–rich, polyunsaturated fatty acid–based nanoemulsion formulation was developed for effective encapsulation of this peptide to overcome absorption limitation within the nasal cavity and for enhancing nose-to-brain delivery. Nanoemulsions are oil-in-water or water-in-oil formulations that can be prepared with various edible oils, and they are versatile in the types of payloads and targeting capabilities that can be made possible (Singh et al., 2017).

Materials and Methods

Statistical Analysis

The primary statistical analysis was performed using GraphPad Prism [version 7.00; La Jolla, CA (www.graphpad.com)].

The in vitro transfection studies in LPS model were analyzed using one-way analysis of variance (Tukey's multiple comparison test). The in vivo transfection studies in an LPS rodent model of neuroinflammation were analyzed using the Student's t test to compare different treatment groups. For the MRI studies, statistical Student's t tests were performed on the percentage change in longitudinal relaxation time (T_1) values for major brain regions and 172 specific brain regions in each subject. The t test statistics using a 95% confidence level ($^*P < 0.05$) and a 99% confidence level ($^{**}P < 0.001$), two-tailed distributions, and heteroscedastic variance assumptions were performed.

Materials

High omega-3 fatty acid–containing flaxseed oil was provided by Jedwards International (Quincy, MA). Lipoid E80 was purchased from Lipoid GmbH (Ludwigshafen, Germany). Tween 80, stearylamine, and CSA peptide were purchased from Sigma-Aldrich (St. Louis, MO). The nasal septum carcinoma cell line (RPMI 2650) was purchased from American Type Culture Collections (Rockville, MD). The media and reagents necessary for cell culture primers, and polymerase chain reaction (PCR) reagent were purchased from Thermo Fisher Scientific (Waltham, MA). Transwell companion plates and inserts were purchased from BD Biosciences (San Jose, CA). Gadolinium (III) chloride hexahydrate, diethylenetriamine pentaacetic acid (DTPA), Arsenazo dye, and LPS (*Escherichia coli* 0111:B4) were purchased from Sigma-Aldrich. All other chemicals were procured from Thermo Fisher Scientific and were used as received.

Preparation and Characterization of CSA Nanoemulsions

Oil-in-water nanoemulsions were prepared by the sonication method. Positively charged nanoemulsions were prepared using stearylamine, whereas the negatively charged nanoemulsions were prepared using the same ingredients except without stearylamine. The negative surface charge on the nanoemulsions was due to egg phosphatidylcholine (Lipoid E80) and Tween 80, which aids by creating polyethylene glycol surface modification. CSA was dissolved in ethanol (50 mg/ml) to prepare a CSA stock solution. The oil phase was prepared by mixing flax seed oil with the drug in ethanol. The aqueous phase was prepared by using egg phosphatidylcholine (Lipoid E80) and Tween 80. In the case of positively charged nanoemulsions, stearylamine was also added to the aqueous phase. The oil phase (oil-drug mixture) was vortexed for a few minutes, and ethanol was completely evaporated using liquid nitrogen. The oil phase was then added slowly to the aqueous phase containing lipoid E80 and Tween 80 with or without stearylamine. After adding oil phase to the aqueous phase, the mixture was homogenized and then ultrasonicated in an ice bath to prevent the sample from excessive heating and to protect the peptide from degradation. Because CSA has limited solubility in water, an aqueous suspension formulation of CSA (CSA-S) was formulated as an appropriate control for CSA nanoemulsions. The CSA-S was prepared by mixing CSA in ethanol with egg phosphatidylcholine in distilled water. Tween 80 was added to the mixture in the same proportion as for the nanoemulsion formulation. A screen was performed to select a correct type and percentage of surfactants/excipients (Tween 80, deoxycholic acid, L-histidine, stearylamine) for the nanoemulsion formulation, with the goal of achieving a particle size of less than 250 nm with low polydispersity.

Nanoemulsion formulations were characterized for particle size with the use of dynamic light scattering on a Brookhaven Instruments Corporation (Holtsville, NY) 90 Plus ZetaPALS Particle Size Analyzer at a 90° fixed angle and at 25°C. Nanoemulsions were diluted with deionized water, and the z-average of the oil droplet hydrodynamic diameter as well as the polydispersity index (PDI) were recorded. During the measurement, the average particle count rate was maintained between 50 and 500 kcps. The ZetaPALS instrument was also used to measure the surface charge (zeta potential) of the nanoemulsions. Measurements were made on diluted nanoemulsions, as described above. The refractive index of the nanoemulsion was at 1.33 and the viscosity was at 1.0 cps to mimic the values for pure water.

Drug loading, encapsulation efficiency, and stability were evaluated using the high-performance liquid chromatography (HPLC) method. The extent of loading of CSA nanoemulsions (i.e., the amount of peptide incorporated in internal oil phase of nanoemulsion) was determined using HPLC. The CSA nanoemulsion was diluted with 100% methanol, and 50 μl of the dissolved nanoemulsion was injected in HPLC. Mobile phase A (1% trifluoroacetic acid in water) and mobile phase B (1% trifluoroacetic acid in acetonitrile) were pumped through the Agilent (Santa Clara, CA) Zorbax 300StableBond-C18 Column (particle size, 3.5 μm; 4.6 × 100 mm) at a flow rate of 1 ml/min. A gradient of 30% mobile phase B to 100% mobile

phase B was achieved in 8 minutes, and peptide elution was monitored at a wavelength of 215 nm. For encapsulation efficiency, 0.5 ml of a diluted (100×) formulation was transferred to polyvinylidene fluoride Ultrafree-CL Centrifugal Filter units having 0.1 μ pore size (catalog #UFC40VV25; EMD Millipore, Bedford, MA) and centrifuged at 5000*g* for 15 minutes at 4°C. The aqueous phase that moved through the filter into the sample recovery chamber was injected on the HPLC, and the concentration of the peptide was estimated. Encapsulation efficiency was calculated based on mass balance. Nanoemulsions samples were studied for stability with respect to its uniformity (appearance), particle size, and surface charge at 3 months after storage at 4°C. Drug-loaded nanoemulsions were tested for chemical stability up to 3 months after storage at 4°C.

Permeability, Intracellular Uptake, and Cytotoxicity Evaluation in RPMI 2650 Cells

In vitro studies were performed to understand the mechanistic aspects of nasal absorption/permeability. The aim was to understand the permeability of CSA nanoemulsions compared with the solution formed through nasal epithelial cells before performing the in vivo studies. We have evaluated a number of different in vitro nasal permeability models to determine the barrier properties of the nasal mucosa for efficient delivery. RPMI 2650 nasal epithelial cells were selected for the studies because it is the most commonly used human cell line for nasal drug transport studies and originates from an anaplastic squamous cell carcinoma of the nasal septum (Bai et al., 2008). These cells also displayed consistent growth, high stability throughout continued culturing in vitro, higher transepithelial electrical resistance (TEER) values at the air-liquid interface, reproducibility of results, and ease of both access and maintenance (Moore and Sandberg, 1964). Furthermore, these cells are also known to form interconnected tight junction proteins zonula occludens-1, occluding, claudin-1, and E-cadherin (Bai et al., 2008).

For the permeability studies, RPMI 2650 cells were cultured on inserts in flat-bottomed 12-well plates at a density of 300,000 cells/cm^2. Media were changed every third day until 7 days. The cells were then grown on the air-liquid interface for another 7 days. The TEER value was measured after 14 days, and the cells were treated with a 20 μM concentration of either positively charged CSA nanoemulsion (NE-SA) or negatively charged CSA nanoemulsion (NE-T), and with CSA solution in 0.5% dimethylsulfoxide (DMSO) Hanks' balanced salt solution 1× buffer (T-CSA) at similar concentrations ($n = 3$). The permeability of CSA formulations was assessed from apical to basolateral (AB) direction and vice versa at 37°C for 2 hours with shaking at 50 rpm. The samples were quantitated by the liquid chromatography (LC) tandem mass spectrometry (MS) method.

To evaluate and compare the intracellular uptake of CSA nanoemulsions and CSA in solution, RPMI 2650 cells were cultured on six-well plates at a density of 300,000 cells/cm^2. Media were changed the next day before treating cells with a 20 μM concentration of either NE-SA or NE-T and T-CSA ($n = 3$). After 3 and 24 hours of incubation, cells in each well were washed three times with cold 1× PBS (pH 7.4) and were lysed using cell lysis buffer. CSA was extracted from the cell lysate using a solvent extraction method. Briefly, 500 μl of acetonitrile was added and, after mixing cell debris, was collected and centrifuged, and 800 μl of supernatant was aliquoted out in new tubing and dried by solvent evaporation. The dry sample was redispersed with 200 μl of a 50:50 composition of LC-MS media buffer B (5 mM ammonium formate in methanol) and acetonitrile. Samples were run on an LTQ LC-MS (Thermo Fisher Scientific), and quantitation was performed based on the calibration curve. The amount of total protein was determined using a BCA Protein Assay Kit (Thermo Fisher Scientific). The percentage dose uptake per milligram of protein was calculated.

For the cytotoxicity studies, RPMI 2650 cells were seeded at a density of 5000 cells/well in 96 wells. After 72 hours, cells were rinsed and incubated with 10 and 20 μM concentrations of NE-SA or NE-T and with T-CSA ($n = 8$). Treatment with cell media was used as a negative control, and treatment with branched polyethyleneimine (molecular weight, 10 kDa), a cationic cytotoxic polymer at 10 μg/ml was used as a positive control. After 48 hours of treatment time, the cells were rinsed with media and 50 μl of 5 mM MTT [3-(4,5-dimethylthiazol-2-yl)-2,5-diphenyl tetrazolium bromide] reagent in phosphate-buffered saline (PBS) (pH 7.4) (Life Technologies Vybrant MTT Cell Proliferation Assay Kit; Thermo Fisher Scientific) was added. During the incubation period of 1 hour at 37°C, MTT dye was converted to formazan by the live cells. DMSO 200 μl was added to the plates, and, after shaking for a few minutes, the absorbance value was measured at 490 nm. In this assay, the absorbance value is directly proportional to the live cells. The percentage of cell viability was calculated from the absorbance values relative to those of untreated cells.

In Vitro Evaluation of Anti-Inflammatory Effects of CSA Nanoemulsion in LPS-Stimulated Macrophages

To quantitatively assess the potential anti-inflammatory therapeutic effect of the CSA-loaded nanoemulsion, the levels of proinflammatory cytokines tumor necrosis factor-α (TNF-α), interleukin (IL)-1β, IL-6, and the inducible nitric oxide synthase (iNOS) were measured at the mRNA level by reverse-transcription PCR in LPS (Sigma-Aldrich)-stimulated J774A.1 macrophages. Cells were counted and plated on day 1 in a six-well microplate at 50,000 cell density, and after day 4 cells were first treated with either CSA-S or with the positively charged CSA nanoemulsion (CSA-NE) formulation for 4 hours ($n = 3$) at a concentration of 1 μg/ml. After 4 hours of pretreatment, cells were stimulated with 100 ng/ml LPS. Prior to confirming 100 ng/ml as the final LPS dose, several concentrations of LPS at several time points were experimented on in cells, and 100 ng/ml LPS for 6 hours resulted in significant upregulation of target cytokines. After 6 hours of stimulation, cells were washed and collected by centrifugation at 5000*g* for 10 minutes. A cell pellet was used for RNA extraction using the manufacture protocol (Roche, Indianapolis, IN). The extracted RNA was quantified and about 400 ng of RNA was used for cDNA synthesis (TaqMan Reverse Transcription Reagent). The second step of quantitative PCR was performed using TaqMan probes for specific cytokines using the TaqMan Gene Expression Master Mix. β-Actin was used as an internal control. A standard curve was also prepared using cDNA from the LPS-treated cells. TNF-α levels were measured at protein level by using a TNF-α–specific enzyme-linked immunosorbent assay kit (R&D Systems, Minneapolis, MN) (data not shown).

Qualitative Brain Distribution of Intranasal Nanoemulsion in Rats Using MRI

The purpose of this comparative study was to compare, the uptake of gadolinium (Gd^{3+})-encapsulated nanoemulsion (Gd^{3+}-NE) and *N*-methylglucamine salt of the gadolinium complex of diethylenetriamine pentaacetic acid aqueous solution (Magnevist; Bayer, Whippany, NJ) into the brain using MRI, which is being considered the gold standard in the diagnosis of brain disorders and brain imaging (Lux and Sherry, 2018). Gd^{3+} contrast agent for MRI has unpaired electrons that interact with surrounding water molecules to decrease their T_1 values. MRI can measure T_1 by creating a magnetic field that reverses the magnetization of the sample, then recording the time required for the spin directions to realign in their equilibrium positions. A decrease in the T_1 relaxation time from the baseline T_1 value of the target tissue allows MRI instruments to better distinguish contrast from surrounding environment (Lux and Sherry, 2018).

Synthesis of Phosphatidylethanolamine-DTPA-Gd^{3+} Conjugate. To prepare the nanoemulsion with Gd^{3+} ions for contrast enhancement in MRI, we synthesized and purified the phosphatidylethanolamine (PE)-DTPA-Gd^{3+} (PE-DTPA-Gd^{3+}) conjugate. To chelate Gd^{3+} ions for MRI contrast, PE was conjugated with DTPA using a previously published protocol (Sandip et al., 2006).

Triethylamine (60 μl) was added to egg PE (200 mg), which was dissolved in 8 ml of chloroform. The solution was then added dropwise

to a 1 mM DTPA anhydride solution (800 mg in 40 ml of DMSO), and the mixture was stirred for 3 hours under nitrogen atmosphere in an open flask. The suspension was dialyzed overnight using a 2-kDa molecular-weight cutoff membranes (Spectrum Spectra/Por; Repligen, Rancho Dominguez, CA) to eliminate free DTPA, and the resulting conjugate was lyophilized. Gadolinium trichloride (37 mg; equivalent to 40.0 mmol) dissolved in 0.2 ml of water was added dropwise to the DTPA-PE mixture (dissolved in 40 ml of DMSO) and stirred for 1 hour, followed by dialysis with water using a 2-kDa membrane. The water was changed three times a day. The final DTPA-PE-Gd mixture was lyophilized for 2–3 days. Free gadolinium is a known toxin and a heavy metal, and may contribute toward total gadolinium concentration. The amount of free gadolinium in the complex was checked using the 200 μl of 0.2 mM Arsenazo dye. Arsenazo III binds to metal ions forming an Arsenazo-metal ion complex, which was qualitatively analyzed by the color change. The final product was stored at −80°C and was used to prepare the formulations.

Formulation of Gd^{3+}-Labeled Nanoemulsions for MRI. Gd^{3+}ions containing nanoemulsions were prepared by a high-energy ultrasonication method. As described above, DTPA-PE-Gd complex (0.5 mmol Gd^{3+}), Lipoid E80 (48 mg), Tween 80 (8 mg), and stearylamine (8 mg) were added to water (1.6 ml), and the mixture was stirred for 30 minutes to achieve complete dissolution of these excipients. Separately, 0.4 g of flaxseed oil was taken in a glass vial. The two phases were then heated on a hot plate at 70°C for 3–5 minutes. The aqueous phase was added to the oil phase, and the mixture was sonicated at 21% amplitude and 50% duty cycle (Vibra Cell VC 505; Sonics and Materials Inc., Newtown, CT) for 10 minutes, resulting in the formation of the nanoemulsion. The mean particle hydrodynamic diameter and zeta potential of the nanoemulsions droplets was measured as described in the section "Preparation and Characterization of CSA Nanoemulsions" with a 200-fold dilution of the formulation with distilled water.

MRI was used to determine the T_1 of the Gd^{3+}-containing nanoemulsions. According to the exponential decay function, the magnetization is at T_1 is $(1-\frac{1}{e})$, or approximately one-third less than the equilibrium magnetization. Hence, by extrapolating the time at this magnetization, it was possible to determine the T_1 relaxation rate. Nanoemulsion was diluted into Eppendrof tubes and run through a Biospin Bruker BioSpec 7.0-T/20-cm bore UltraShielded Refrigerated Horizontal Magnet (Bruker, Billerica, MA). The Magnevist solution, which is used as a control, was also diluted and run for the measurement of in vitro T_1 values.

Experimental Design for MRI Studies. All of the animal experiments discussed here were approved by the Northeastern University Institutional Animal Care and Use Committee. Female Sprague-Dawley rats (210–230 g) were obtained from Charles River Laboratories (Cambridge, MA) and were kept on a 12-hour light/dark cycle with ad libitum access to food and water. All of the described animal experiments were approved by the Northeastern University Institutional Animal Care and Use Committee. Rats were acclimated to their environment for 2 days before the experiments. All MRI experiments were carried out at room temperature. Experiments were conducted using a BioSpec 7.0-T/20-cm UltraShielded Refrigerated horizontal magnet (Bruker) and a 20-G/cm magnetic field gradient insert (i.d., 12 cm). Radiofrequency signals were sent and received with the quad-coil electronics built into the animal restrainer. The rats ($n = 6$) were administered PE-DTPA-Gd^{3+} containing nanoemulsion formulations at 0.02 mmol/kg (40 μl of total nanoemulsion or Magnevist solution using the 50 μl Hamilton syringe, 5-μl volume administered in alternative nostrils and total volume administered in 20 minutes). Rats were placed in a head restrainer for imaging at various time points after the dosing. Predosing images of the brain regions of the rat were also collected for comparison of T_1 values.

Anatomic MR Scans. At the beginning of each imaging session, a high-resolution anatomic data set was collected using the RARE (Rapid Imaging with Refocused Echoes) pulse sequence [20 slices; 1 mm; field of view (FOV), 3.0 cm; 256 × 256; repetition time (TR) 2.5 seconds; echo time, 12.4 milliseconds; number of excitations, 3]. Variable TR images were acquired using RARE pulse sequence (echo time, 12.5 milliseconds; TR, 460, 900, 1400, 2800, and 6000 milliseconds) Images were acquired with an FOV of 3 cm^2, a data matrix of 128 × 128 × 20 slices, and a thickness of 1 mm. T_1 measurements were computed using ParaVision 5.1 software (Bruker) by fitting the absolute signal at a particular TR. The T1 map data were collected at 128 × 128 (x-y) and 22 slices. Voxel resolution was 0.234 × 0.234 mm in plane and a slice thickness of 1.2 mm. The FOV was 30 × 30 × 26.4 cm. Isoflurane (2.5%–3%) was constantly supplied throughout the imaging session using a nose cone to maintain the respiratory rate between 40 and 60 breaths/min. During image acquisition, the respiratory rate was monitored continuously over the entire imaging period using a small animal heating and monitoring system (SA Instruments, Stonybrook, NY). After the first baseline scan (a predose scan) of the whole brain, rats were administered a total dose of 0.1 mmol/kg based on body weight. After the dosing was finished within 20 minutes, MR scans were commenced to capture the postdosing time points of 30, 60, and 90 minutes.

MR Data Analysis and Image Processing. Each subject at different time points of 0, 30, 60, and 90 minutes was registered to a 3D segmented and annotated rat brain atlas (Ekam Solutions LLC, Boston, MA). The alignment process was facilitated by an interactive graphic user interface, EVA (Ekam Solutions LLC). The affine registration involved translation, rotation, and scaling in all three dimensions independently. The matrices that transformed the subject's anatomy to the atlas space were used to embed each slice within the atlas. All transformed pixel locations of the anatomy images were tagged with the segmented atlas regions, creating a fully segmented representation of each subject. Each subject is segmented into 172 distinct brain regions. T_1 parameter values for each region of interest was computed based on each segmented map.

Percent change decrease in T_1 values at each time point and in each major regions and specific regions was calculated at t = 30-, 60-, and 90-minute time points as described:

$$\%\ Change\ in\ T_1\ value\ of\ ROI\ at\ t = \frac{(T_1\ of\ ROI\ at\ 0\ min - T_1\ of\ ROI\ at\ t\ min) \times 100}{T_1\ of\ ROI\ at\ time\ 0}$$

In Vivo Evaluation of Therapeutic Efficacy of CSA Nanoemulsion in an LPS Rat Model of Neuroinflammation

To evaluate and compare the protective anti-inflammatory effect of CSA in LPS-induced degeneration of nigral dopaminergic neurons, Sprague-Dawley rats were pretreated with 5 mg/kg CSA-S and CSA-NE formulations. Rats were briefly anesthetized using ketamine and xylazine (80 and 20 mg/kg, respectively), and after sedation rats were dosed with 5 mg/kg concentrations of CSA-S and CSA-NE intranasally over a period of 30 minutes using a 20 μl manual micropipette. Rats were pretreated with CSA formulations 3 hours prior to the LPS treatment.

For LPS injection, the Sprague-Dawley rats were deeply anesthetized using isoflurane (2.5%–3%). The head of the animal was shaved and swabbed with 70% isopropyl alcohol and betadine. Rats were then placed in the stereotaxic instrument. Body temperature was maintained throughout the procedure at 38°C using a heating pad (Fintronic USA, San Mateo, CA). A sterile scalpel was used to create a 1- to 2-cm rostral-to-caudal incision on the scalp, and to expose the bregma. Tissue overlying the suture lines was scraped away, and the skull was dried using a dryer. A surgical drill (Dremel, Racine, WI) was then used to create a burr hole (1–2 mm), and stereotaxic coordinates of 4.8 mm posterior to bregma, 1.7 mm lateral to the midline, and 8.2 mm ventral to the surface of the skull were used for

injection into the substantia nigra (SN) region. Rats were dosed with 2 μg of LPS, and cytokine stimulation was evaluated at the 6-hour time point. The needle of a 5-μl syringe (Hamilton, Reno, NV), containing the LPS solution, was then lowered to −8.8 mm ventral to the surface of the skull, and 1 μl of LPS was injected using a motorized microinjection Harvard Apparatus (Holliston, MA) infusion pump at a rate of 0.5 μl/min. After the injection, the needle was kept in place for 2 minutes and then slowly pulled out to minimize efflux. LPS was prepared as a stock solution of 2 mg/ml in sterile PBS (pH 7.4). Each rat received an injection of LPS dissolved in PBS onto the right side of the brain, and the contralateral left side was used as an internal control and was analyzed separately. After LPS injection, rats were returned to a cage, and food and water was supplied. At 6 hours after the LPS injection, the rats were sacrificed, and the brain was collected. Microdissection was performed using the adult rat brain slicer matrix, and 1–2 mm of the slices were dissected. Samples from the SN region were collected from both the injected side and the contralateral side and were frozen immediately. Tissues samples were processed further after homogenization with Qiazol (Thermo Fisher Scientific) to perform RNA extraction. Total RNA was isolated and purified from brain tissue using RNeasy Lipid Tissue Mini Kit as per instructions from Qiagen (Venlo, The Netherlands). The isolated mRNA from the tissue samples described above was quantified by UV spectrophotometry using the NanoDrop Instrument (Thermo Fisher Scientific). A gene quantitation assay using the TaqMan Gene Expression Master Mix and TaqMan Gene Expression Assays from Applied Biosystems (Foster, CA) was performed as per instructions. The samples were run in triplicate, and data were analyzed using the comparative threshold cycle (Ct) method by calculating $\Delta\Delta$Ct values for each treatment, and results were expressed as the percentage of relative expression compared with β-actin as endogenous control and normalized to the untreated animals.

Acute Safety Assessments

To examine safety, the following study was designed for each treatment group as a solution and as a nanoemulsion with controls: body weight monitoring, histopathological evaluation of nasal mucosa, and histopathological evaluation of liver sections.

Changes in Body Weight. Periodic measurements of body weight were performed upon injecting the control (PBS only), CSA-S (5 mg/kg), and CSA-NE (5 mg/kg) formulations via intranasal route of administration on day 0 to day 3. Frequent body weight measurements were made through the course of the study. A total of two animals was used. The results were plotted as the percentage change in body weight as a function of the daily pretreatment administration for all the treatment groups.

Nasal Tissue Histopathology. To evaluate the toxic effect on the nasal mucosa, rats were first dosed with 5 mg/kg concentrations of CSA-S and CSA-NE, and only saline was used as a control. After exsanguination at the time point of 6 hours postadministration, the head was removed from the carcasses. The tissues samples were preserved in formalin fixative until histopathological processing. After fixation and decalcification, four tissue slices were taken at the following levels: (1) immediately posterior to the upper incisor teeth; (2) at the incisive papilla or the anterior nasal cavity; (3) at the premolar or middle part of the nasal cavity; and (4) at the middle of the first molar teeth or posterior part of the nasal cavity. The nasal tissues were processed in a conventional manner. Paraffin-embedded tissues were cut into 5-μm sections and mounted on glass slides, and coverslips were placed on glass slides. Tissue sections were dried and deparaffinized using a xylene substitute followed by decreasing concentrations of ethanol down to purified water. Sections were incubated in hematoxylin, rinsed with water, and incubated with 1% acid alcohol (clearing reagent). Sections were rinsed and incubated with 4% ammonia solution (bluing reagent). Sections were then incubated with eosin followed by dehydration with two changes each in 95% ethanol and 100% ethanol followed by a final change of a xylene substitute. Tissues were then mounted on slides and coverslips were placed on glass slides, and a digital image was captured using a light microscope (n = 2/treatment). Blinded analysis of toxicological profile and tissue damage, if any, was carried out by Dr. Jerry Lyon, a certified veterinary pathologist, at the Tufts University Veterinary School in Grafton, MA.

Liver Tissue Histopathology. Liver tissues samples were collected for histopathological analysis from rats at 3 days after treatment with PBS (control), 5 mg/kg concentrations of CSA-S and CSA-NE formulations via the intranasal route of administration. These tissue samples were preserved in formalin before analysis. Paraffin-embedded tissues were microtomed into 5-μm sections and mounted on glass slides, and a coverslip was placed on top of the tissue sample in each slide. The tissue sections were dried and deparaffinized using a xylene substitute followed by decreasing concentrations of ethanol and finally purified water. Sections were incubated in hematoxylin, rinsed with water, and incubated with 1% acid alcohol (clearing reagent). Sections were rinsed and incubated with a 4% ammonia solution (bluing reagent). Sections were then incubated with eosin followed by dehydration by two changes each in 95% ethanol and 100% ethanol followed by a final change of the xylene substitute. Tissues were mounted on a slide, and a digital image was captured using a light microscopy. Blinded analysis of toxicological profile and tissue damage, if any, was carried out by Dr. Jerry Lyon, a certified veterinary pathologist, at the Tufts University Veterinary School in Grafton, MA.

Results

Preparation and Characterization of CSA Nanoemulsions. The final composition that showed the best particle size distribution for nanoemulsion was found to be 2.5% w/v lipoid E80, 0.2% w/v Tween 80, 0.2% w/v stearylamine, and 20% w/v flaxseed oil (Table 1). The theoretical loadings for positive and negative nanoemulsions were different as CSA had different solubility profiles with and without stearylamine. Both negatively and positively charged formulations were used for comparison in cell transport and tolerability studies.

Permeability, Intracellular Uptake, and Cytotoxicity Evaluation. We were able to use the RPMI 2650 cells for transport studies as they formed a uniform confluent monolayer when cells were grown under an air-liquid interface. The highest TEER values of 200 Ω/cm^2 were observed when cells were seeded at a density of 4×10^5 cells/cm^2 onto a polyethylene terephthalate insert of 0.4-cm^2 surface area with 0.4-μm pore size, which demonstrates the barrier-like properties of the model. RPMI 2650 cells also showed the presence of the tight junction protein zonula occludens-1 (data not shown). Furthermore, the apparent permeability coefficient of the paracellular marker sodium fluorescein was found to be $(8.07 \pm 0.01) \times 10^{-6}$ cm/s, which is an indication of a uniform monolayer (Wengst and Reichl, 2010; Goncalves et al., 2016). The RPMI 2650 cell monolayer was used to assess and compare the transport of the CSA peptide formulations. The delivery of CSA-NE showed an increase in AB transport (582 ± 5 ng/ml) when compared with transport of a CSA solution (100 ± 20 ng/ml) (Fig. 1A). A negatively charged nanoemulsion was unable to show an increase in the transport of CSA. These findings indicating an increase in the transport of CSA via a positively charged nanoemulsion formulation with a simultaneous decrease in the efflux are of immense importance since CSA is an efflux substrate. Intracellular studies performed with CSA peptide showed no major difference between solution or nanoemulsion formulations for the

TABLE 1
Composition and characterization properties of anionic and cationic nanoemulsions formulations of CSA

Formulation	Composition	CSA Initial Loading Concentration	Hydrodynamic Diameter of Oil Droplet	PDI	Zeta Potential	CSA Encapsulation
		mg/ml	nm		mV	%
CSA-encapsulated anionic nanoemulsion (NE-T)	Lipoid E80, Tween 80, and flaxseed oil	25	232 ± 10[a]	0.25 ± 0.06	−33 ± 12	88 ± 10
CSA-encapsulated cationic nanoemulsion (NE-SA)	Lipoid E80, Tween 80, stearylamine, and flaxseed oil	30	272 ± 12	0.3 ± 0.09	57 ± 10	88 ± 13

[a]Mean ± S.D. (n = 4).

early time point of 3 hours. However, nanoemulsion at a later time point of 24 hours showed an increase in uptake, but the T-CSA solution showed a decrease over time. Nanoemulsion showed a potential for enhanced uptake in cells at a later time point, and uptake seems to not saturate over time. There was no clear difference for intracellular uptake for the NE-SA formulation (positively charged) and the NE-T formulation (negatively charged) (Fig. 1B).

CSA nanoemulsion formulations with positively and negatively charged showed enhanced tolerability up to a concentration of 20 μM compared with the solution form of the peptide, which showed viability of only 75% under similar conditions (Fig. 1C). This shows that the CSA nanoemulsions are less cytotoxic compared with the solution form of CSA. Because the positively charged nanoemulsion showed overall enhanced cell transport, this formulation was selected for further comparative studies and was labeled as NE-SA for all further studies.

Anti-Inflammatory Effects of CSA in LPS-Stimulated Macrophages. The potential anti-inflammatory effect of CSA-NE in J774A.1 macrophages was evaluated by measuring the levels of TNF-α, IL-1β, IL-6, and iNOS proinflammatory cytokines, after stimulation with LPS toxin. First, we determined the cytokines, which showed stimulation with LPS. Previously, we have seen that the stimulation of cells with LPS at a time point of 4–6 hours results in high stimulation of these cytokines (Jain and Amiji, 2012). We selected 4 hours as a pretreatment time point for the CSA-NE and CSA-S. All four

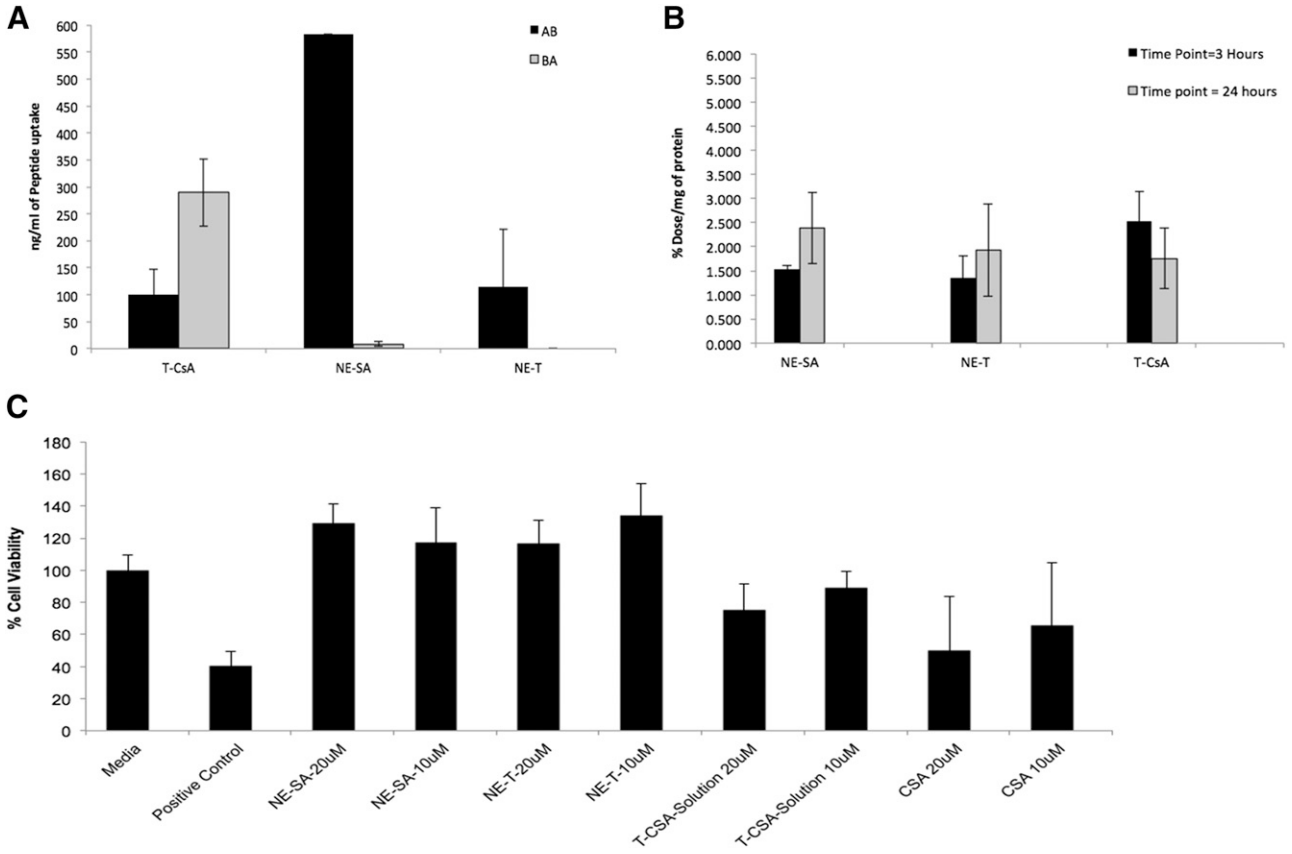

Fig. 1. (A) T-CSA (cellular transport of cyclosporine in solution), NE-SA (positively charged nanoemulsion), and NE-T (negatively charged nanoemulsion) through RPMI 2650 monolayer cells from AB direction and BA (data presented as mean ± S.D.; n = 3). (B) Intracellular uptake of T-CSA, NE-SA, and NE-T in RPMI 2650 cells at 3 and 24 hours (data are presented as the mean ± S.D.; n = 3). (C) RPMI 2650 cell viability results for CSA nanoemulsion formulations T-CSA, NE-SA, and NE-T at 10 and 20 μM concentrations, respectively, when compared with a solution of CSA at 48 hours. Only media was used as a negative control and treatment with polyethyleneimine was used as a positive control. Data are presented as the mean ± S.D. n = 8.

cytokine standard curves were found to be linear with a good slope value (data not shown). When comparing CSA-S to CSA-NE (1 μg/ml), there was a significant decrease in the mRNA levels of all four cytokines (Fig. 2). Data were plotted by considering the expression of a specific marker as 100% in untreated cells that were not given any treatment. The solution formulation that was tested at this concentration showed less of an effect on the cytokines, possibly because of the reduced uptake and high efflux of the CSA solution, which was evident in the transport studies performed with nasal squamous epithelial cells.

Transport of Gd^{3+}-Labeled Nanoemulsion Using MRI. PE-DTPA-Gd^{3+} complex formed was found to be free of any gadolinium ions when tested with Arsenazo dye. These complexes were further used in the nanoemulsions where the PE-DTPA-Gd^{3+} complex was integrated into the nanoemulsion layer and the Gd^{3+} ion on the surface served as the contrast agent for the MRI studies in vivo (Supplemental Fig. 1). Particle size characterization showed the *z*-average to be 342.4 $\pm$ 21 nm with a PDI of 0.20 and a surface charge of 26.5 $\pm$ 0.833 mV. PE-DTPA-Gd^{3+} ion–containing nanoemulsions were also characterized using in vitro magnetic relaxivity values (Supplemental Fig. 2) relates the concentration of Gd^{3+} with the reciprocal of T_1, a relation that results in a linear line with a slope of 6.58 seconds^{-1} mmol^{-1}. This slope is referred to as R_1 or the magnetic relaxivity and indicated the relative contrast efficiency. The R_1 values of the Gd^{3+}-NE solution were compared with those of the Magnevist solution, which is a commercially marketed contrast agent and served here as the standard basis for comparison. It is clear from Supplemental Fig. 2 that the Gd^{3+}-NE solution significantly reduced the relaxation time relative to pure water and had a higher slope (meaning grater R_1 value) compared with that of Magnevist.

The results in Fig. 3A show the anterior-to-posterior overlay of the rat brain regions, which showed significant changes in T_1 values upon Gd^{3+}-NE solution intranasal delivery. MRI studies of the different major regions of the brain after intranasal administration of Gd^{3+}-NE resulted in a unique and widespread distribution of Gd^{3+}-NE in the brain, as is evident by the significant decrease in T_1 values in the major regions of the brain (Fig. 3B). There was a fast uptake within the first 30 minutes, as observed by a significant drop in T_1 values in most of the regions of the brain except the cerebellum and amygdala. This drop in T_1 values was found to be significant when compared with those of the control group. In the cerebellum, including in the cranial nerves and ventral

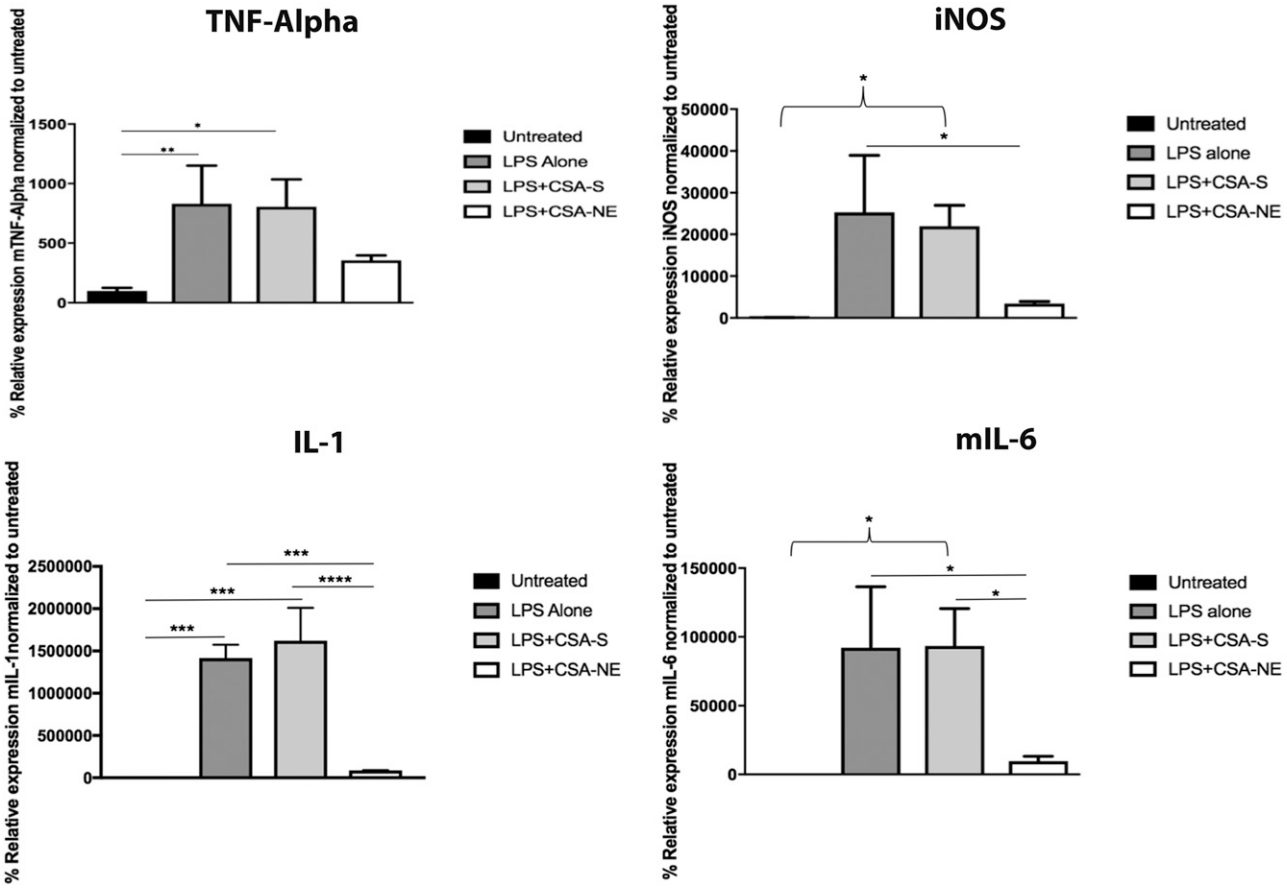

Fig. 2. Inflammatory marker TNF-α–, iNOS-, IL-1–, and IL-6–specific mRNA results showing transcript expression in the J774A.1 macrophage cell line. With LPS treatment (positive control), there was a significant increase in mRNA expression of cytokines TNF-α (**$P < 0.001$), iNOS (*$P < 0.05$), IL-1 (***$P < 0.0001$), and IL-6 (*$P < 0.05$). With NE-SA (a positively charged CSA nanoemulsion) treatment, there was a significant decrease in expression of inflammatory cytokines iNOS (*$P < 0.05$), IL-1 (***$P < 0.001$), and IL-6 (*$P < 0.05$), compared with LPS-alone treatment. There was a significant decrease in the expression of IL-1 (****$P < 0.0001$) and IL-6 (*$P < 0.05$) for the NE-SA–treated group when compared with CSA-S (CSA in solution)–treated group. Untreated cells were used as a negative control. The values are reported as the mean $\pm$ S.D. (n = 3). All statistics were performed using one-way analysis of variance (Tukey's multiple comparison test).

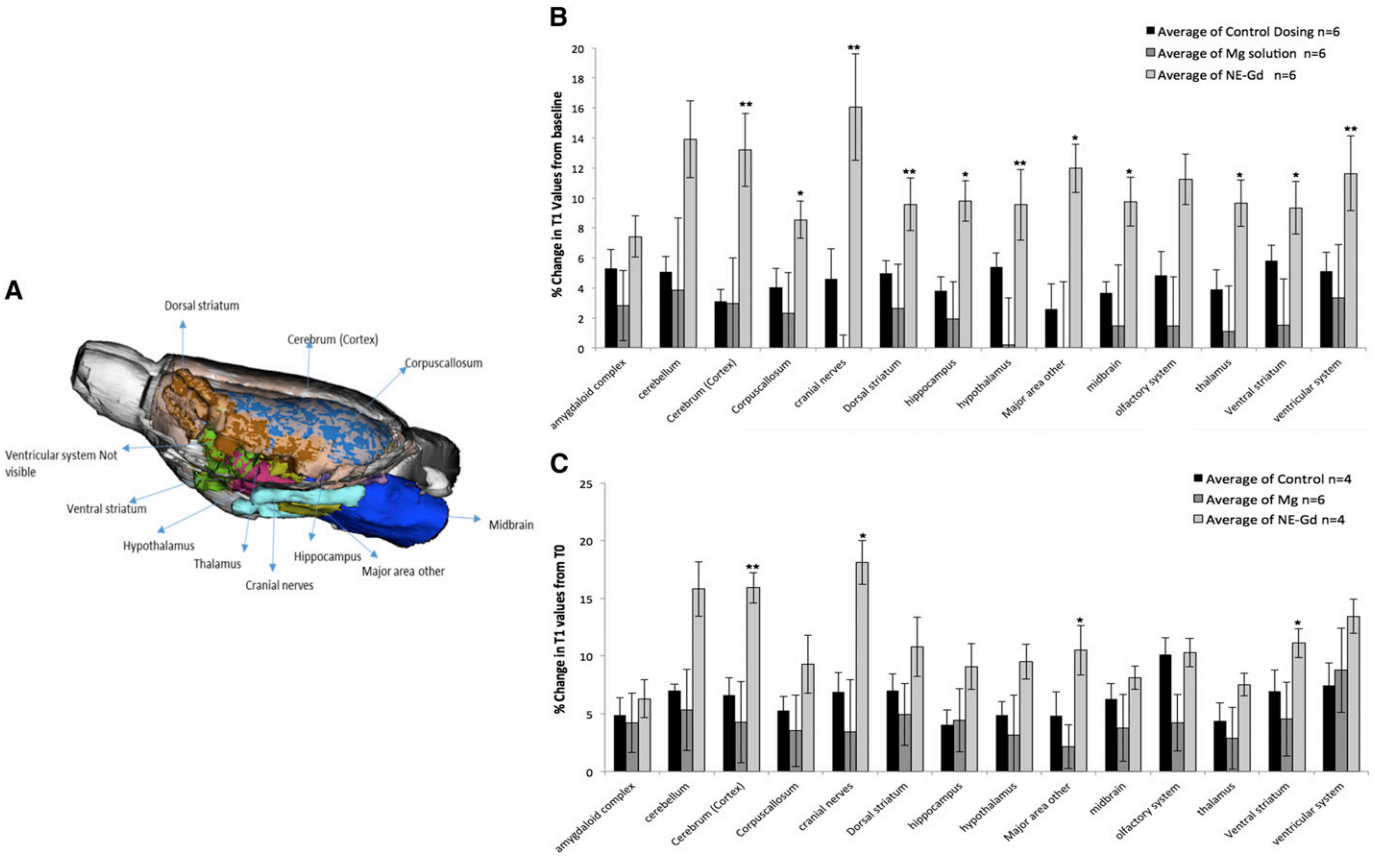

Fig. 3. (A) Highlighted major brain regions in an anterior-to-posterior overlay in a rat brain atlas showing a significant change in T_1 values for nanoemulsion-Gd (NE-Gd) compared with control or Magnevist at the time point of 25–30 minutes postdose. (B) Gd^{3+} ion–containing nanoemulsion distribution at the time point of 25–30 minutes compared with Magnevist and control in major regions of the brain. There was a significant percentage decrease in T1 values for different brain regions for NE-SA group ($^*P < 0.05$; $^{**}P < 0.001$) compared with control. (C) Nanoemulsion-Gd distribution at the time point of 55–60 minutes compared with Magnevist and control in major regions of the brain. There was a significant decrease in T_1 values for the NE-SA group ($^*P < 0.05$) compared with the control group. Student's t tests were performed on the percentage change in T_1 values for major brain regions and 172 specific brain regions in each subject. The t test statistics using 95% ($^*P < 0.05$) and 99% ($^{**}P < 0.001$) confidence levels, two-tailed distributions, and heteroscedastic variance assumptions were performed.

striatum, there was a significant difference in the relaxivity values at 55–60 minutes after administration (Fig. 3C). When the data were analyzed for the 172 specific regions of the brain, we found 22 of 172 brain regions showing higher and significant uptake for the Gd^{3+}-NE solution compared with control (Fig. 4). Magnevist distribution in the brain was found to be lower than the Gd^{3+}-NE distribution (as evident from the higher decrease in T_1 changes due to Gd^{3+}-NE), suggesting a possibility that nanoemulsion are being taken up by an intracellular endocytosis process or through the trigeminal pathways where they could lead to higher uptake in different and distant regions of the brain. Further, the nanoemulsion shows a signal in different regions of the brain for a longer time period compared with Gd in solution (i.e., Magnevist).

Evaluations, of the Anti-Inflammatory Effects of CSA-NE in an LPS Rat Model of Neuroinflammation. We used the LPS-induced model and performed quantitative PCR analysis to evaluate the profiles of cytokines in SN regions upon treatment with control and nanoemulsion formulations for CSA. Both the injectable site SN and contralateral side SN were dissected from the brain 6 hours after LPS injection. Samples were then processed for total RNA extraction, cDNA synthesis, and subsequent PCR amplification. From Fig. 5, the relative percentages of cytokine levels for different treatment groups after 3 hours of pretreatment with CSA can be seen. As indicated in Fig. 5, the levels of proinflammatory cytokines for the LPS-induced rats on the right side of the SN (Fig. 5, LPS only R) were found to be significantly higher than those of the non-LPS control saline group (Fig. 5, Control Saline R). For instance, the percentages for the relative expression of TNF-α, iNOS, and IL-6 after LPS stimulation were found to be 19,177% ± 269%, 1876% ± 725%, and 2300% ± 576%. CSA delivered as a solution formulation was found to be slightly effective in exerting a therapeutic effect at this time point, where TNF-α reached 14,223% ± 7305%, with higher variability within the levels. The considerably lower effect of the CSA solution was also found in the in vitro studies conducted in LPS-stimulated macrophages. On the other hand, CSA-NE significantly lowered the levels of TNF-α (2786% ± 328%) compared with those in the LPS-induced group and the CSA solution group, which emphasizes the importance of a nanoemulsion-based delivery system. The levels of other cytokines IL-2 and IL-6 were also found to be lowered; however, the results were not significantly different. IL-2 is another cytokine specifically downregulated by CSA and has been studied and found to be upregulated by T lymphocytes. Upon LPS stimulation, apart from microglia there is evidence that lymphocytes can also infiltrate the

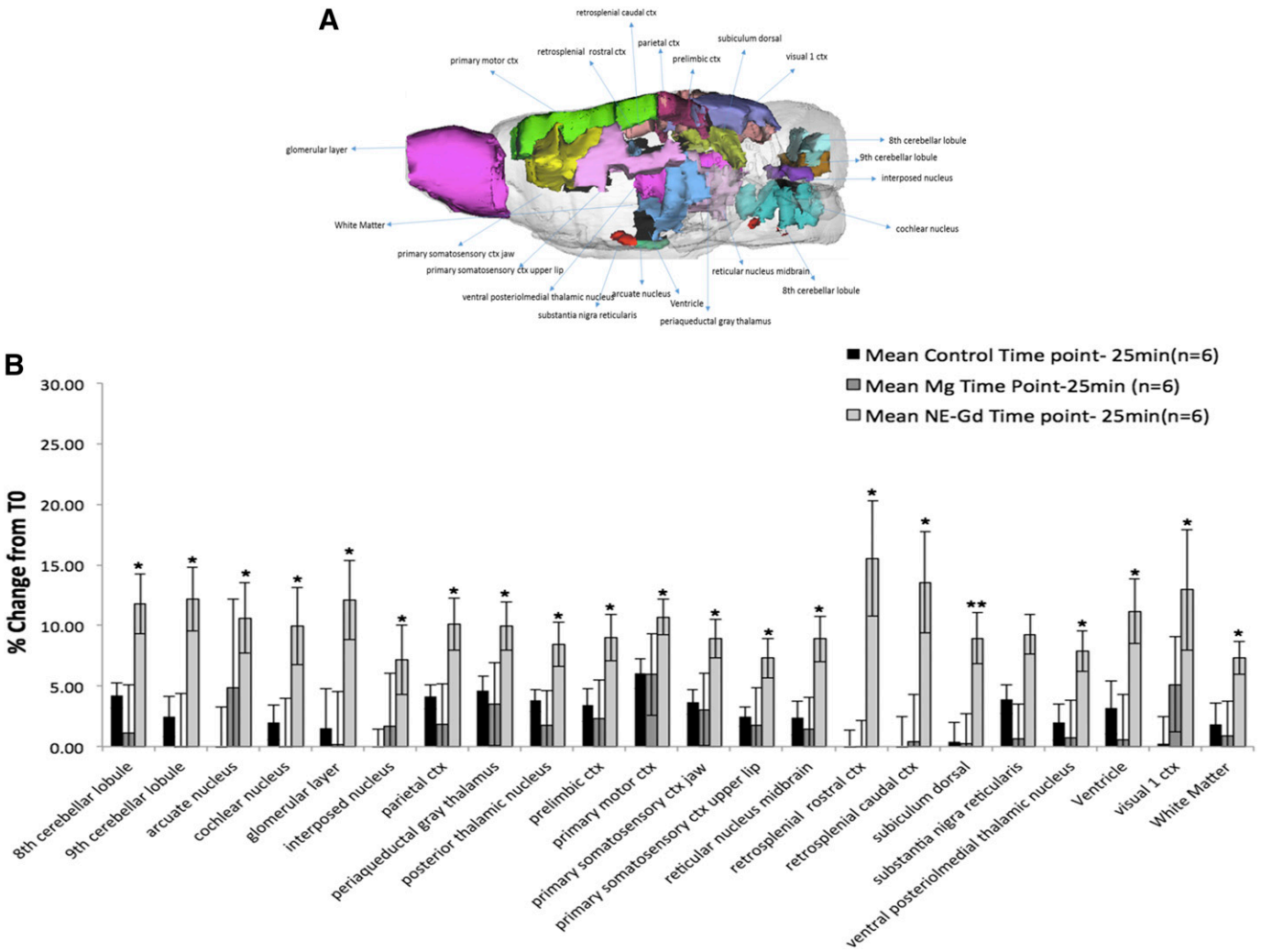

Fig. 4. (A) Representative overlay of rat brain regions showing the distribution of Gd contrast agent in different specific regions after intranasal administration. (B) Nanoemulsion-Gd (NE-Gd) distribution at the time point of 25–30 minutes compared with Magnevist and control in specific regions of the brain. There was a significant decrease in T_1 values for the NE-SA–treated group for different brain regions ($^*P < 0.05$) compared with the control group. Student's t tests were performed on the percentage change in T_1 values for major brain regions and 172 specific brain regions of each subject. The t test statistics using a 95% ($^*P < 0.05$) and 99% ($^{**}P < 0.001$) confidence levels, two-tailed distributions, and heteroscedastic variance assumptions were performed. ctx, cortex.

injection site. CSA-NE showed inhibition of the IL-2 gene expression, which is known to be involved in the maintenance of regulatory T cells and is also involved in the differentiation plus survival of T cells. The therapeutic effects observed on the IL-2 cytokine were based on the inhibition of the endogenous levels. It was later found that LPS is not an effective stimulator of IL-2 levels, and, hence, if the levels of IL-2 are considerably increased using other types of toxins, we might be able to observe a higher inhibition effect on this cytokine. Overall, the CSA-NE treatment was found to be considerably effective in inhibiting the expression of cytokines, including TNF-α, and was found to be slightly effective in downregulating other cytokines, like IL-2 and IL-6, though not significant. There was no effect of CSA-NE or CSA-S on iNOS levels.

Acute Safety Assessments. There was a slight difference in the body weights of rats treated with the three groups: PBS control, CSA-S, and CSA-NE. After day 1, all the groups gained weight except for the CSA-S group. Rats in the CSA-NE group showed a steady gain in weight after day 1 (Fig. 6A). These results suggest that the nanoemulsion formulations were well tolerated in rats.

Based on the histopathological report, all of the normal structures of the nasal cavities were identified, and no significant pathology is identified in any of the sections for any of the animals. Upon a closer view of the respiratory and the olfactory mucosal linings of the nasal cavity, there were no significant changes found in either of the epithelial cells lining the nasal cavity (Fig. 6B). As shown in (Fig. 6C), there was moderate periacinar and diffused hepatocellular vacuolation. Occasional multifocal aggregates of cells were present in portal areas consistent with extramedullary hematopoiesis (Li et al., 2003). Mild extramedullary hematopoiesis and lipid vacuolation are considered as common incidental findings in the liver and are not thought to be related to the treatment as they were also observed in control naive animals (R24) (Li et al., 2003). Hence, the histopathological findings of liver tissue for the groups treated are consistent with what is regarded as being within normal limits.

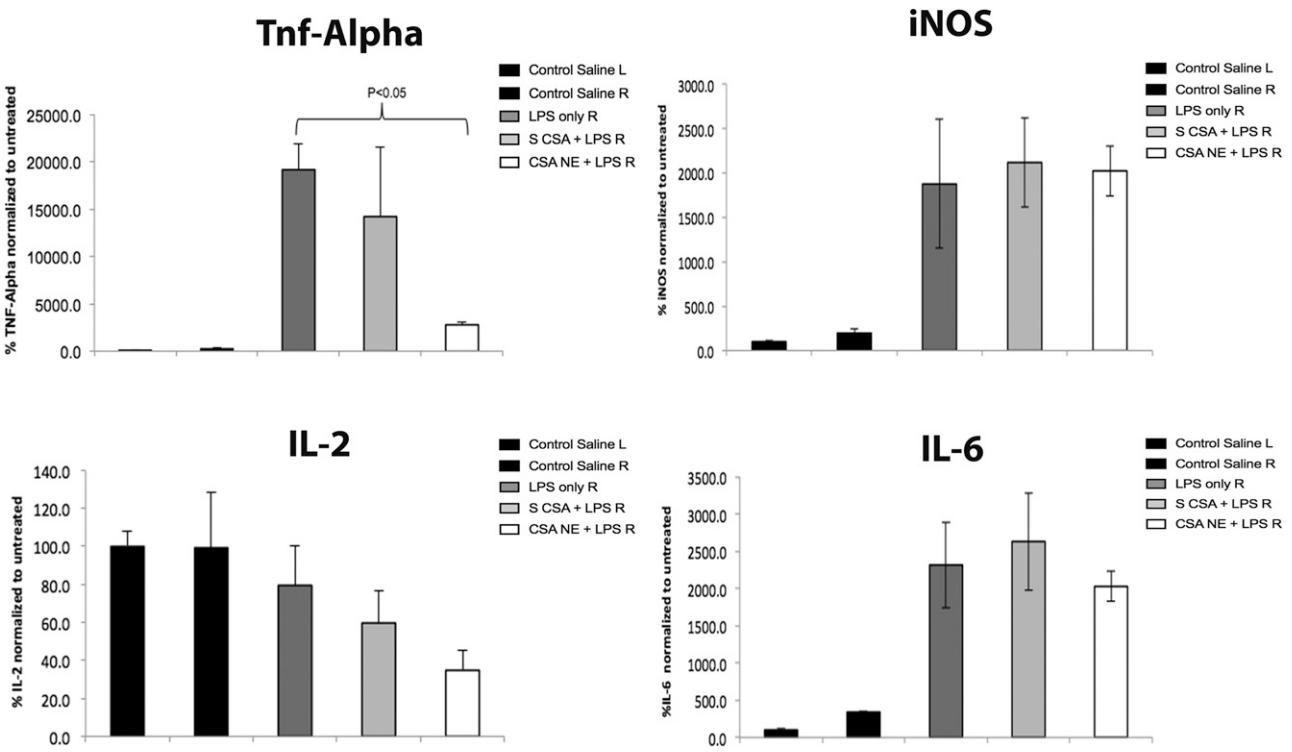

Fig. 5. Inflammatory marker TNF-α–, iNOS-, IL-2–, and IL-6–specific mRNA results showing transcript expression in the SN region of rat brain after treating rats with only saline, only LPS, CSA-NE + LPS, and CSA-S + LPS. There was a significant decrease in TNF-α expression after treatment with NE-SA (positively charged nanoemulsion) compared with LPS alone. Saline-treated rats were used as negative controls and LPS-treated rats were used as positive controls ($^*P < 0.05$). The values are reported as the mean ± S.E.M. ($n = 5$). Statistical analysis was performed using a Student's t test for the comparison of various groups.

Discussion

Peptides have been investigated as potential agents for the treatment of various CNS disorders. There is an unmet need for therapeutic strategies to ensure the efficient delivery of peptide drugs to the brain (Yi et al., 2014). Recently, intranasal delivery has gained a lot of attention for the direct delivery of drugs to the brain and CNS (Djupesland et al., 2014). In the previous study (Yadav et al., 2015), we have shown that nanoemulsions of cyclosporine are capable of showing higher brain targeting upon intranasal delivery. Nanoemulsions, when compared with solution formulation, showed enhanced uptake in different regions of the brain with lower systemic exposure upon intranasal administration (Yadav et al., 2015). This study was designed to further evaluate and understand the benefits of using a nanoemulsion delivery system for the intranasal delivery of CSA peptide to the brain. In the *Introduction*, We discussed a few limiting factors of nasal absorption, such as physical barriers or the poor permeability of large–molecular weight drugs, enzymatic barriers of nasal mucosa, and efflux transporters. In vitro models of nasal mucosa have been used in excised tissue samples, primary cell cultures, or immortalized cell lines (Wengst and Reichl, 2010). However, excised human tissue is hard to obtain, and using animal tissue introduces high variability in addition to questions regarding species differences. Hence, in an attempt to understand the barriers for CSA nasal administration, we used the RPMI 2650 cell model to study the cell transport and found that the positively charged CSA-NE solution showed higher cell transport from the AB direction. Also the transport from the basolateral-to-apical (BA) direction was reduced, which signifies reduction in the efflux of CSA. Furthermore, an increase in intracellular uptake was found for CSA-NE formulations especially at a later time, which further confirms that cyclosporine transport through an efflux transporter is reduced by using an oil-in-water nanoemulsion particulate system.

CSA-NE systems were found to be well tolerated in the murine macrophage cells and hence were considered safe to be used further for in vivo evaluations. To understand the benefit of nanoemulsion formulations, we further compared the anti-inflammatory effect of CSA in J774A.1 macrophages, which were stimulated by LPS. These cells were used as a surrogate cell model because of the limited supply/source of primary microglia. Bacterial LPS has been extensively used in models studying inflammation because it mimics many inflammatory effects of cytokines, such as the upregulation of cytokines like TNF-α, IL-1β, or IL-6. LPS is the most abundant component within the cell wall of Gram-negative bacteria. It can stimulate the release of inflammatory cytokines in various cell types, leading to an acute inflammatory response toward pathogens (Abe et al., 1995). When tested in J774A.1 cells, CSA-NE showed a reduction in cytokine stimulation upon LPS stimulation, which is most likely because of the higher transport and intracellular concentration of CSA when compared with CSA-S. Nanoemulsions overall showed benefits over solutions of CSA because of their potential in avoiding efflux, which in turn leads to high intracellular accumulation compared with the solution form of the peptide. Because of their positive inhibitory effect on the various cytokines, we further evaluated these formulations in vivo in an LPS-stimulated neuroinflammation model.

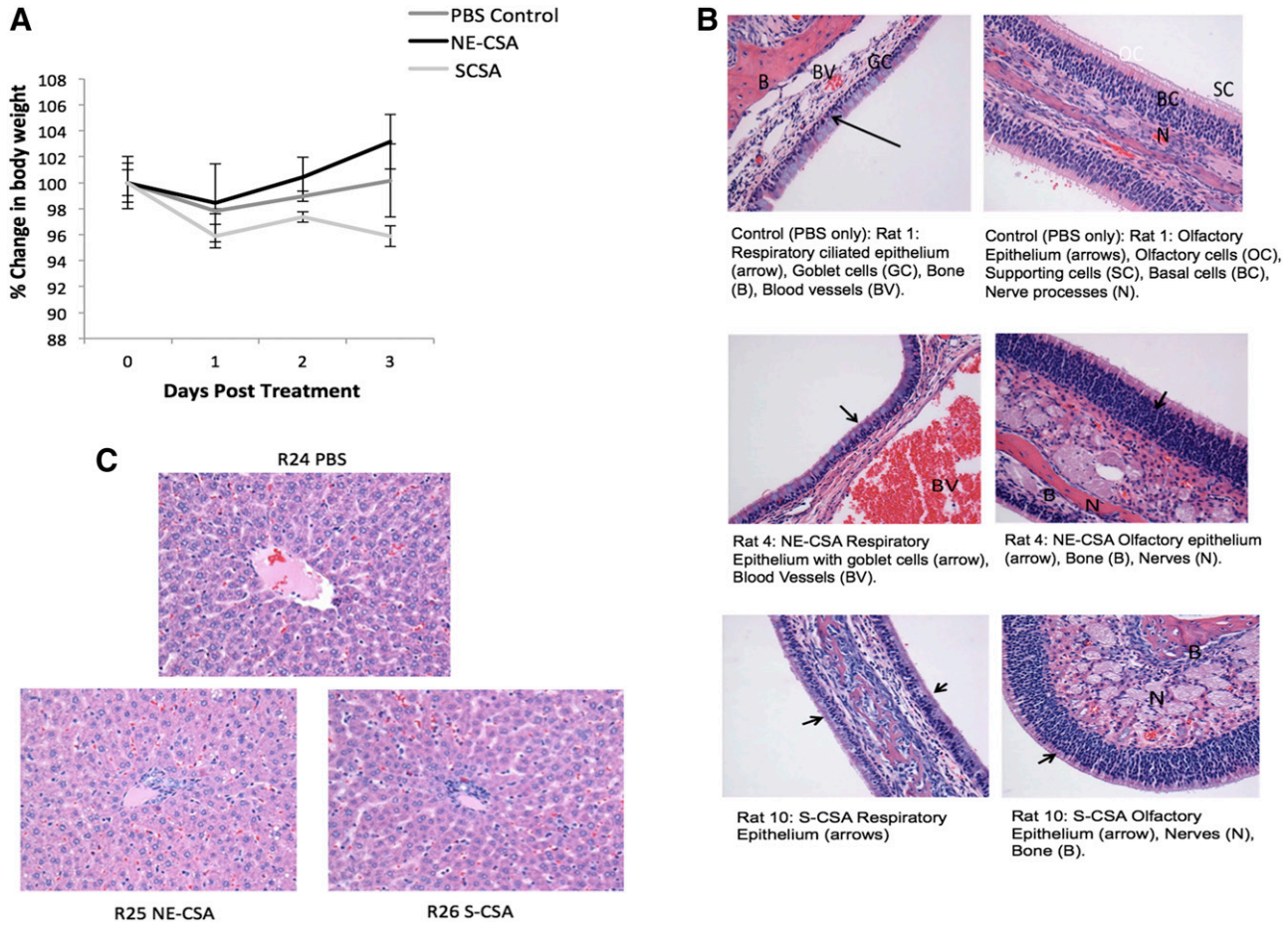

Fig. 6. (A) Body weight measurements to determine the safety/tolerability profile upon single intranasal administration of the control (saline) and positively charged CSA nanoemulsion (CSA-NE). (B) The values are reported as the percentage change in body weight as a function of the pretreatment weight of rats. (C) Histology of nasal respiratory, olfactory epithelium, and liver after intranasal dosing of CSA formulations (NE-SA and CSA-S).

Furthermore, to assess and understand the potential advantages of using a nanocarrier-based system rather than aqueous formulations for intranasal delivery to the brain, we designed an MRI-based uptake study. Based on the distribution study, we demonstrated that a Gd^{3+} ion–containing nanoemulsion can reach multiple sites within the brain as early as 30 minutes after the intranasal administration. In some brain regions, there was a significant change in T_1 values of up to 10%–15%. It is evident that some of the areas where higher T_1 changes were observed are not in close proximity of olfactory bulbs. The wide distribution of CSA in the brain can be attributed to the olfactory neuronal pathway and trigeminal nerve pathway (Mittal et al., 2014). The distribution of CSA from olfactory bulbs to other parts of the brain as observed from MRI can be attributed to diffusion that can also be driven by perivascular pump. This could be driven by arterial pulsation in the brain (Mittal et al., 2014). Furthermore, the distribution and uptake were found to be significantly different than that for the uptake of Magnevist aqueous solution. This potentially is due to the low residence time of aqueous solutions in the nasal cavity and hence the lower chance for nasal absorption by the olfactory epithelium because of rapid clearance via a mucociliary clearance mechanism. We have demonstrated that intranasal application of Gd^{3+}-NE results in rapid delivery to multiple regions of the CNS that are known to be involved in the pathogenesis of neurodegenerative diseases.

For the therapeutic benefit of CSA in the brain, we tested these formulations in vivo in a rat LPS model of neuroinflammation. The amount of LPS used has previously been reported to cause the stimulation of various cytokines together with damage to nigral dopaminergic neurons and astrocytes in vivo (Liu et al., 2000; Tomás-Camardiel et al., 2004). Our therapeutic efficacy studies conducted in an LPS-induced model of neuroinflammation showed that intranasal delivery of a nanoemulsion incorporating a anti-inflammatory molecule like cyclosporine was capable of inhibiting the activated cytokines to a greater extent over the solution formulation treatments. The better effect observed with a nanoemulsion again highlights the importance of using nanoemulsions, which have shown better brain-targeting efficiency based on the distribution study performed earlier (Yadav et al., 2015). The deleterious role of activated microglia together with mediators (cytokines, complement factors) under conditions of inflammation in the CNS is becoming more evident and is found to be closely associated with degenerating neurons (McGeer and McGeer, 1995). The therapeutic approach of using anti-inflammatory measures for targeted delivery to the CNS could really be beneficial for slowly progressing diseases of the brain, which are associated with inflammation.

In addition to evaluating delivery and therapeutic efficacy, it was of utmost importance to monitor the safety and tolerability of formulations delivered through the intranasal route. Because local toxicity to the nasal mucosa will be detrimental, we looked into the impact of using nanoemulsion formulations on nasal tissues along with liver tissues. Our safety results showed no major tolerability problem for intranasal dosing with nanoemulsion.

Conclusions. Peptide delivery to the brain has been a major challenge because of various barriers. We have used the intranasal delivery route to directly deliver peptide to the brain, overcoming the systemic circulation. We have shown efficient delivery of anti-inflammatory peptide (CSA) using cationic nanoemulsion. We showed significant inhibition of proinflammatory cytokines both in vitro and in vivo in the LPS-stimulated model of neuroinflammation. Further, nanoemulsion showed enhanced uptake in various regions of the brain upon intranasal delivery when compared with solution formulation. Nanoemulsion formulations were found to be safe based on acute safety studies performed in rats. Our results indicate that nanoemulsions enhance nose-to-brain uptake of peptide and further are capable of providing therapeutic effects. Further studies considering the behavioral impact of anti-inflammatory effects when delivered via the intranasal route would guarantee its clinical usefulness as a noninvasive therapeutic approach for the treatment of neuroinflammation, a common denominator in many different types of chronic neurodegenerative diseases.

Acknowledgments

We thank Dr. Barbara Caldarone and Paul Lorello at the Harvard Medical School Neuro-Discovery Center in Boston, MA, for providing training in stereotaxic apparatus use and surgery for microinjection in rats. We also thank Dr. Jerry Lyon at the Tufts University Veterinary School for assistance with the tissue histology and analysis. In addition, we thank Srujan Kumar Gandham for assistance with the neuroinflammation model development and in vivo experiments.

Authorship Contributions

Participated in research design: Yadav, Kulkarni, Ferris, and Amiji.

Conducted experiments: Yadav and Pawar.

Contributed new reagents or analytic tools: Kulkarni, Ferris, and Amiji.

Performed data analysis: Yadav, Pawar, and Kulkarni.

Wrote or contributed to the writing of the manuscript: Yadav, Pawar, and Amiji.

References

Abe K, Irie T, and Uekama K (1995) Enhanced nasal delivery of luteinizing hormone releasing hormone agonist buserelin by oleic acid solubilized and stabilized in hydroxypropyl-beta-cyclodextrin. *Chem Pharm Bull (Tokyo)* **43**:2232–2237.

Bai S, Yang T, Abbruscato TJ, and Ahsan F (2008) Evaluation of human nasal RPMI 2650 cells grown at an air-liquid interface as a model for nasal drug transport studies. *J Pharm Sci* **97**:1165–1178.

Barakat NS, Omar SA, and Ahmed AA (2006) Carbamazepine uptake into rat brain following intra-olfactory transport. *J Pharm Pharmacol* **58**:63–72.

Benedict C, Hallschmid M, Hatke A, Schultes B, Fehm HL, Born J, and Kern W (2004) Intranasal insulin improves memory in humans. *Psychoneuroendocrinology* **29**:1326–1334.

Chow HH, Anavy N, and Villalobos A (2001) Direct nose-brain transport of benzoylecgonine following intranasal administration in rats. *J Pharm Sci* **90**: 1729–1735.

Djupesland PG, Messina JC, and Mahmoud RA (2014) The nasal approach to delivering treatment for brain diseases: an anatomic, physiologic, and delivery technology overview. *Ther Deliv* **5**:709–733.

Foltin RW and Haney M (2004) Intranasal cocaine in humans: acute tolerance, cardiovascular and subjective effects. *Pharmacol Biochem Behav* **78**:93–101.

Gabryel B and Bozena J (2009) Effect of FK506 and cyclosporine A on the expression of BDNF, Tyrosine kinase B and p75 neurotrophin receptors in astrocytes exposed to simulated ischemia in vitro. *Cell Biol Int* **33**:739–748.

Göldner FM and Patrick FM (1996) Neuronal localization of the Cyclophilin A protein in the adult rat brain. *J Comp Neurol* **372**:283–293.

Gonçalves VSS, Matias AA, Poejo J, Serra AT, and Duarte CMM (2016) Application of RPMI 2650 as a cell model to evaluate solid formulations for intranasal delivery of drugs. *Int J Pharm* **515**:1–10.

Hashizume R, Ozawa T, Gryaznov SM, Bollen AW, Lamborn KR, Frey WH II, and Deen DF (2008) New therapeutic approach for brain tumors: intranasal delivery of telomerase inhibitor GRN163. *Neuro-oncol* **10**:112–120.

Jain S and Amiji M (2012) Tuftsin-modified alginate nanoparticles as a noncondensing macrophage-targeted DNA delivery system. *Biomacromolecules* **13**: 1074–1085.

Jogani VV, Shah PJ, Mishra P, Mishra AK, and Misra AR (2008) Intranasal mucoadhesive microemulsion of tacrine to improve brain targeting. *Alzheimer Dis Assoc Disord* **22**:116–124.

Kosfeld M, Heinrichs M, Zak PJ, Fischbacher U, and Fehr E (2005) Oxytocin increases trust in humans. *Nature* **435**:673–676.

Li X, Elwell MR, Ryan AM, and Ochoa R (2003) Morphogenesis of postmortem hepatocyte vacuolation and liver weight increases in Sprague-Dawley rats. *Toxicol Pathol* **31**:682–688.

Liu B, Jiang J-W, Wilson BC, Du L, Yang S-N, Wang J-Y, Wu G-C, Cao X-D, and Hong J-S (2000) Systemic infusion of naloxone reduces degeneration of rat substantia nigral dopaminergic neurons induced by intranigral injection of lipopolysaccharide. *J Pharmacol Exp Ther* **295**:125–132.

Lu CT, Zhao YZ, Wong HL, Cai J, Peng L, and Tian XQ (2014) Current approaches to enhance CNS delivery of drugs across the brain barriers. *Int J Nanomedicine* **9**: 2241–2257.

Lux J and Sherry AD (2018) Advances in gadolinium-based MRI contrast agent designs for monitoring biological processes in vivo. *Curr Opin Chem Biol* **45**: 121–130.

McGeer PL and McGeer EG (1995) The inflammatory response system of brain: implications for therapy of Alzheimer and other neurodegenerative diseases. *Brain Res Brain Res Rev* **21**:195–218.

Mittal D, Ali A, Md S, Baboota S, Sahni JK, and Ali J (2014) Insights into direct nose to brain delivery: current status and future perspective. *Drug Deliv* **21**:75–86.

Miyata K, Omori N, Uchino H, Yamaguchi T, Isshiki A, and Shibasaki F (2001) Involvement of the brain-derived neurotrophic factor/TrkB pathway in neuroprotecive effect of cyclosporin A in forebrain ischemia. *Neuroscience* **105**:571–578.

Moore GE and Sandberg AA (1964) Studies of a human tumor cell line with a diploid karyotype. *Cancer* **17**:170–175.

Osman MM, Lulic D, Glover L, Stahl CE, Lau T, van Loveren H, and Borlongan CV (2011) Cyclosporine-A as a neuroprotective agent against stroke: its translation from laboratory research to clinical application. *Neuropeptides* **45**: 359–368.

Sandip T, Yi-Meng T, and Mansoor A (2006) Preparation and in vitro characterization of multifunctional nanoemulsions for simultaneous MR imaging and targeted drug dleivery. *J Biomed Nanotechnol* **2**:217–224.

Santos JB and Schauwecker PE (2003) Protection provided by cyclosporin A against excitotoxic neuronal death is genotype dependent. *Epilepsia* **44**:995–1002.

Sheehan J, Eischeid A, Saunders R, and Pouratian N (2006) Potentiation of neurite outgrowth and reduction of apoptosis by immunosuppressive agents: implications for neuronal injury and transplantation. *Neurosurg Focus* **20**:E9.

Singh Y, Meher JG, Raval K, Khan FA, Chaurasia M, Jain NK, and Chourasia MK (2017) Nanoemulsion: concepts, development and applications in drug delivery. *J Control Release* **252**:28–49.

Snyder SH, Sabatini DM, Lai MM, Steiner JP, Hamilton GS, and Suzdak PD (1998) Neural actions of immunophilin ligands. *Trends Pharmacol Sci* **19**:21–26.

Tomás-Camardiel M, Rite I, Herrera AJ, de Pablos RM, Cano J, Machado A, and Venero JL (2004) Minocycline reduces the lipopolysaccharide-induced inflammatory reaction, peroxynitrite-mediated nitration of proteins, disruption of the blood-brain barrier, and damage in the nigral dopaminergic system. *Neurobiol Dis* **16**:190–201.

Wengst A and Reichl S (2010) RPMI 2650 epithelial model and three-dimensional reconstructed human nasal mucosa as in vitro models for nasal permeation studies. *Eur J Pharm Biopharm* **74**:290–297.

Westin U, Piras E, Jansson B, Bergström U, Dahlin M, Brittebo E, and Björk E (2005) Transfer of morphine along the olfactory pathway to the central nervous system after nasal administration to rodents. *Eur J Pharm Sci* **24**: 565–573.

Yadav S, Gattacceca F, Panicucci R, and Amiji MM (2015) Comparative biodistribution and pharmacokinetic analysis of cyclosporine-A in the brain upon intranasal or intravenous administration in an oil-in-water nanoemulsion formulation. *Mol Pharm* **12**:1523–1533.

Yi X, Manickam DS, Brynskikh A, and Kabanov AV (2014) Agile delivery of protein therapeutics to CNS. *J Control Release* **190**:637–663.

Address correspondence to: Mansoor Amiji, Northeastern University, 360 Huntington Avenue, 140 TF, Boston, MA 02115. E-mail: m.amiji@northeastern.edu